NUMERICAL RESULTS FOR VLF MODE CONVERSION IN THE EARTH-IONOSPHERE WAVEGUIDE

Interim Report No. 712

R. A. Pappert, R. R. Smith, L. R. Shockey

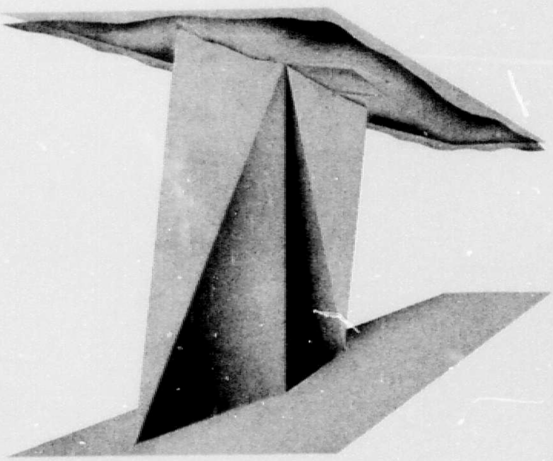

NAVAL ELECTRONICS LABORATORY CENTER
SAN DIEGO, CALIFORNIA 92152

15 April 1971
Prepared for DEFENSE ATOMIC SUPPORT AGENCY
on DASA Subtask HB 042

NELC Problem M402

41

DOCUMENT CONTROL DATA - R & D

(Security classification of title, body of abstract and indexing annotation must be entered when the overall report is classified)

1. ORIGINATING ACTIVITY (Corporate author)

Naval Electronics Laboratory Center
San Diego, California 92152

2a. REPORT SECURITY CLASSIFICATION
Unclassified

2b. GROUP

3. REPORT TITLE

NUMERICAL RESULTS FOR VLF MODE CONVERSION IN THE EARTH-IONOSPHERE WAVEGUIDE

4. DESCRIPTIVE NOTES (Type of report and inclusive dates)

Research Report

5. AUTHOR(S) (First name, middle initial, last name)

Richard A. Pappert, Robert R. Smith and Linda R. Shockey

6. REPORT DATE	7a. TOTAL NO. OF PAGES	7b. NO OF REFS
12 April 1971	40	10

8a. CONTRACT OR GRANT NO.
DASA MIPR 71-555

b. PROJECT NO.

c. DASA Subtask HB 042

d.

9a. ORIGINATOR'S REPORT NUMBER(S)

Interim Report No. 712

9b. OTHER REPORT NO(S) (Any other numbers that may be assigned this report)

10. DISTRIBUTION STATEMENT

Distribution of this document is unlimited.

11. SUPPLEMENTARY NOTES

12. SPONSORING MILITARY ACTIVITY

Defense Atomic Support Agency

13. ABSTRACT

Numerical results are presented for several mode conversion models which allow for the inhomogeneity and anisotropy of the ionosphere. It is concluded that reflections associated with propagation across the terminator do not significantly affect mode conversion. It is shown that significant departure between mode conversion and WKB mode sums can occur when propagating across the terminator even for transition thicknesses as great as 1000 km. Numerical results are compared with the experimental modeling results of the American Nucleonics Corporation.

14 KEY WORDS	LINK A		LINK B		LINK C	
	ROLE	WT	ROLE	WT	ROLE	WT
VLF Propagation						
Waveguide Modes						
Fortran Program						
Mode Conversion						

NUMERICAL RESULTS FOR VLF MODE CONVERSION IN THE EARTH-IONOSPHERE WAVEGUIDE

Interim Report No. 712

R. A. Pappert, R. R. Smith*

and L. R. Shockey

PROPAGATION TECHNOLOGY DIVISION
NAVAL ELECTRONICS LABORATORY CENTER
SAN DIEGO, CALIFORNIA 92152

April 1971

Prepared for DEFENSE ATOMIC SUPPORT AGENCY
on DASA Subtask HB 042

NELC Problem M402

*Now at Undersea Research & Development Center, Transducer and Array Systems Division, San Diego, California 92132

Distribution of this document is unlimited.

ABSTRACT

Numerical results are presented for several mode conversion models which allow for the inhomogeneity and anisotropy of the ionosphere. It is concluded that reflections associated with propagation across the terminator do not significantly affect mode conversion. It is shown that significant departure between mode conversion and WKB mode sums can occur when propagating across the terminator even for transition thicknesses as great as 1000 km. Numerical results are compared with the experimental modeling results of the American Nucleonics Corporation.

INTRODUCTION

This is the second report concerned with VLF mode conversion in the earth ionosphere waveguide under both ambient and disturbed conditions. In this report we concentrate principally on illustrative results for three mode conversion models. The models fall broadly into two categories. In Model I (see reference 1) the strengths of a truncated set of modes are adjusted in such a way as to synthesize a unit amplitude wave in a given mode emerging from the transition region. In Model II a unit amplitude wave in a given mode incident on the junction is decomposed into a truncated set of modes passing through and emerging from the junction. These models, with reflections included in a semiquantitative way, are applied only to the case of abrupt transitions. From a comparison of the results for the two models for the abrupt transition we have drawn the following conclusions:

i) Model II is to be preferred to Model I because of superior convergence of the mode conversion coefficients with mode truncation.

ii) As far as day-night transitions are concerned, reflections, do not significantly affect mode conversion.

Because of ii) above, the third model treated is Model II without reflections, but generalized to handle an arbitrary transition with complete allowance for the inhomogeneity and anisotropy of the ionosphere. A documentation of the associated program will be given in a subsequent report.

Most of the results presented in Section III are based on Model III. Included in the latter are comparisons with experimental modeling studies conducted by the American Nucleonics Corporation.[2,3] Formulas used in the calculation of the results for Models II and III are summarized in the following section. Formulas for Model I are given in reference 1. In Section IV the conclusions are briefly presented.

II. MATCHING BOUNDARY CONDITIONS

Suppose that the propagation path in the x direction has been broken up into slabs as indicated below

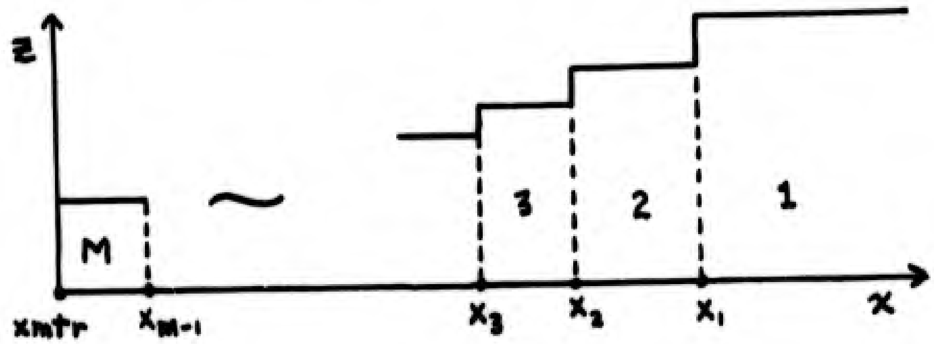

where the variable ionosphere is assumed to be between receiver and transmitter. As a preliminary to the discussion in this section we define the following quantities

$$G_\ell^p = \frac{1}{N_\ell^p}\begin{pmatrix} e_{y\ell}^p \\ e_{z\ell}^p \\ h_{y\ell}^p \\ h_{z\ell}^p \end{pmatrix}, \quad \tilde{G}_\ell^p = \frac{1}{N_\ell^p}\begin{pmatrix} h_{z\ell}^{*p} \\ -h_{y\ell}^{*p} \\ -e_{z\ell}^{*p} \\ e_{y\ell}^{*p} \end{pmatrix}, \tag{1}$$

$$N_\ell^p = \left[2\int_{-\infty}^{\infty} \left(h_{z\ell}^p e_{y\ell}^p - e_{z\ell}^p h_{y\ell}^p \right) dz \right]^{1/2}. \tag{2}$$

In these equations e and h are height gains associated with the electric and magnetic field strengths respectively (with h_y at the ground normalized to unity). The superscript denotes slab number, the y, z subscripts denote the component of the field, the subscript k denotes the mode number and the asterisk denotes the complex conjugate. It can be shown that for propagation transverse to a geomagnetic meridian the integral

$$\int_{-\infty}^{\infty} (\tilde{G}_k^p)^\dagger \, G_m^p \, dz = \delta_{km} = \begin{cases} 0, & k \neq m \\ 1, & k = m \end{cases}, \tag{3}$$

where the dagger denotes the adjoint. Extension of (3) to allow for a general azimuth of propagation involves a generalization of G. Although this generalization is straight forward,[4] it is not required here since the results presented in Section III are restricted to cases for which (1) and (3) apply (i.e. propagation transverse to a geomagnetic meridian).

Suppose now that a unit amplitude wave in mode k propagates in the positive x direction in slab M. Ignoring reflections the continuity of tangential field components at x_p yields

$$\sum_j a_{jk}^{p+1} H_0^2(K S_j^{p+1} x_p) G_j^{p+1} = \sum_j a_{jk}^p H_0^2(K S_j^p x_p) G_j^p . \tag{4}$$

Here H_o^2 represents the Hankel function of the second kind and S_j is the sine of the ground eigenangle for mode j propagating in the positive x direction and K is the free space wave number. The coefficients a_{jk}^p may be interpreted as the amplitude for mode j in slab p which results from a unit amplitude wave in mode k traveling in the positive x direction in slab M. Multiply (4) through by $(\tilde{G}_m^p)^\dagger$ integrate over all z and use (3). This gives

$$a^p_{mk} = \frac{1}{H^2_0(KS^p_m x_p)} \sum_j a^{p+1}_{jk} H^2_0(KS^{p+1}_j x_p) I^{p,p+1}_{mj}$$

$$\approx \sqrt{S^p_m}\, e^{jKS^p_m x_p} \sum_j \frac{a^{p+1}_{jk}}{\sqrt{S^{p+1}_j}} e^{-jKS^{p+1}_j x_p} I^{p,p+1}_{mj}, \tag{5}$$

where

$$I^{p,p+1}_{mj} = \int_{-\infty}^{\infty} (\tilde{G}^p_m)^\dagger G^{p+1}_j \, dz. \tag{6}$$

Equations (5) are to be supplemented with the conditions

$$a^M_{jk} = \delta_{jk}. \tag{7}$$

Observe that if k = 1, 2, 3, ..., N then (5) along with (7) suffice to determine N coefficients a^p_{jk} for each p. To normalize the E_z field in terms of dB/(μv/m-kw) the a^p_{jk} need only be multiplied by

$$\frac{0.03248\ K}{2\sqrt{f}} \left(\frac{N^M_k\ S^p_j}{N^p_j\ S^M_k} \right)^{1/2} \lambda(M, k), \tag{8}$$

where K is the free space wave number in inverse km, f the frequency in kHz and λ(M, k) the complex vertical dipole excitation factor for the vertical electric field[5] for mode k in the M^{th} slab. With the understanding, then, that the a^p_{jk} are multiplied by the factor (8), the total vertical electric field in slab p is

$$E^p_z = \frac{1}{\sqrt{\sin(x_p/a)}} \sum_k \sum_j a^p_{jk} e^{-jKS^p_j x_p} \frac{dB}{\mu v/m\text{-}kw}, \tag{9}$$

where a is the earth's radius.

Numerical results based on (9) will be given in Section III. Results will also be given for the total conversion coefficient, A_{jk}, defined here as the ratio of vertical E emerging from the junction in mode j to the value entering the junction in mode k (apart from the geometrical spreading factors). In our notation it is given by

$$A_{jk} = \sqrt{\frac{S_j^1}{S_k^M}} \; \frac{a_{jk}^1}{a_{kk}^M} \, e^{jK(S_k^M x_{M-1} - S_j^1 x_1)} . \tag{10}$$

Although it may not be evident from (10), A_{jk} is independent of junction location. Also, it includes excitation factor effects associated with compression or dilation of the field due to effective height changes in the guide.

In addition to results based on (9) and (10) we will also give some results including reflection from an abrupt step subject to the assumption of isotropy. For completeness, the formulas for this specialized case are summarized below. Matching tangential electric and magnetic fields at x_1 yields

$$H_0^2(KS_k^2 x_1)\, h_{yk}^2 + \sum_\ell r_{\ell k} H_0^1(KS_\ell^2 x_1)\, h_{y\ell}^2$$
$$= \sum_\ell a_{\ell k}^1 H_0^2(KS_\ell^1 x_1)\, h_{y\ell}^1 , \tag{11}$$

$$H_0^2(KS_k^2 x_1)\, e_{zk}^2 - \sum_\ell r_{\ell k} H_0^1(KS_\ell^2 x_1)\, e_{z\ell}^2$$
$$= \sum_\ell a_{\ell k}^1 H_0^2(KS_\ell^1 x_1)\, e_{z\ell}^1 . \tag{12}$$

Multiply (11) through by e^1_{zm} and (12) through by h^1_{ym} and integrate each of the resultant equations over all z. This gives

$$a^1_{mk}\, H^2_0(KS^1_m x_1) = H^2_0(KS^2_k x_1)\, J^{1,2}_{mk} + \sum_\ell r_{\ell k}\, H^1_0(KS^2_\ell x_1)\, J^{1,2}_{m\ell}, \tag{13}$$

$$a^1_{mk}\, H^2_0(KS^1_m x_1) = H^2_0(KS^2_k x_1)\, I^{1,2}_{mk} - \sum_\ell r_{\ell k}\, H^1_0(KS^2_\ell x_1)\, I^{1,2}_{m\ell}, \tag{14}$$

where

$$J^{1,2}_{m\ell} = \int_{-\infty}^{\infty} e^1_{zm}\, h^2_{y\ell}\, dz \; ; \; I^{1,2}_{m\ell} = \int_{-\infty}^{\infty} h^1_{ym}\, e^2_{z\ell}\, dz. \tag{15}$$

Equations (13) and (14) may be manipulated to give

$$a^1_{mk}\, H^2_0(KS^1_m x_1) = \tfrac{1}{2}\Big[H^2_0(KS^2_k x_1)(J^{1,2}_{mk} + I^{1,2}_{mk}) + \sum_\ell r_{\ell k}\, H^1_0(KS^2_\ell x_1)(J^{1,2}_{m\ell} - I^{1,2}_{m\ell})\Big] \tag{16}$$

$$\sum_\ell r_{\ell k}\, H^1_0(KS^2_\ell x_1)(J^{1,2}_{m\ell} + I^{1,2}_{m\ell}) = H^2_0(KS^2_k x_1)(I^{1,2}_{mk} - J^{1,2}_{mk}) \tag{17}$$

Corresponding to a truncated set of N modes, (16) and (17) represent 2N equations in 2N unknowns. Equation (17) shows that the $r_{\ell k}$ are determined by differences of nearly equal small quantities and (16) shows that the influence of the $r_{\ell k}$ on the a_{mk} comes about only after multiplying the $r_{\ell k}$ by a small number depending upon the difference of the J and I integrals. This simple example illustrates the sensitivity of the reflection coefficients, $r_{\ell k}$, to the height gain integrals and in turn the rather minor role they would be expected to play in determining the conversion coefficients a_{mk}. Calculations based on (16) and (17) bear out the latter assertion and results will be given which suggest that reflections can be ignored in many instances. In those rare occasions when reflections may be important, it still remains to determine whether or not they may be calculated with sufficient accuracy. This clearly depends upon the accuracy with which the height gain functions and their associated integrals may be determined along with the necessary matrix inversions required.

III. RESULTS

In this section numerical results are given for the three models discussed in the introduction. Table 1 shows results for an abrupt transition between two isotropic homogeneous ionospheres which has been studied by Wait (ω_r is the ratio of the square of the circular plasma frequency to the electron collision frequency). The numbers apply to the total mode conversion coefficient A_{jk} (conversion from mode k to mode j) defined by (10). The first column shows Wait's results.[3] The latter have been modified so as to be consistent with our equation (10). The second column shows our results with reflections included via (16) and (17) (our Model II). In addition to the inclusion of reflection, our method differs from Wait's in the sense that allowance is made for tail off of the height gains in the ionosphere. Also, the height gains are obtained by numerical integration,[7] and the integrals of the height gains are obtained numerically using a Romberg[8] integration scheme (in the corresponding evaluations Wait makes use of properties of Airy functions). It will be seen that the results in columns one and two are in excellent agreement (e.g. differences in mode sums based on the numbers in columns 1 and 2 would be indistinguishable). The rather small values of A_{jj} (j = 1, 2, 3) result from the field expansion effect associated with going from the height h_1 = 70 km to the height h_2 = 90 km. Column 3 shows results with the program of reference 1 (Model I). Serious departure from the results of columns 1 and 2 will be noted, particularly for those coefficients which involve k = 3.

TABLE 1

$\alpha_r = 2 \times 10^{5}\ SEC^{-1}$ $h_1 = 70km$ $h_2 = 90km$ $f = 20kHz$

MODE CONVERSION COEFFICIENTS(A_{JK})

	WAIT	3 MODES MODEL II	3 MODES MODEL I	6 MODES MODEL I
J = 1 K = 1	0.4680 $\angle$ .0686	0.4730 $\angle$ .0614	0.4867 $\angle$ .0649	0.4590 $\angle$ .05841
J = 1 K = 2	0.1247 $\angle$ 3.2312	0.1242 $\angle$ -3.0792	0.1498 $\angle$ -3.047	0.1047 $\angle$ -3.1314
J = 1 K = 3	0.0808 $\angle$ .0532	0.0765 $\angle$ -.0064	0.3090 $\angle$ 0.1861	0.0404 $\angle$ -.3970
J = 2 K = 1	0.6552 $\angle$ -.0696	0.6603 $\angle$ -.0644	0.6242 $\angle$ -.0744	0.6979 $\angle$ -.0538
J = 2 K = 2	0.6366 $\angle$ .0078	0.6334 $\angle$ -.0116	0.7018 $\angle$ .0079	0.5796 $\angle$ -.0396
J = 2 K = 3	0.2432 $\angle$ 3.1438	0.2295 $\angle$ 3.0914	0.8519 $\angle$ -3.0145	0.1302 $\angle$ 2.7601
J = 3 K = 1	0.1595 $\angle$ 3.0125	0.1670 $\angle$ 3.0476	0.1209 $\angle$ 2.9963	0.2174 $\angle$ 3.0887
J = 3 K = 2	0.5523 $\angle$ .0227	0.5692 $\angle$ .0290	0.4822 $\angle$ .01276	0.6445 $\angle$ .0529
J = 3 K = 3	0.4464 $\angle$ -.0645	0.4358 $\angle$ -.0948	1.2370 $\angle$ .0475	0.3002 $\angle$ -.2970

The fourth column shows again results based on Model I where six modes rather than three modes have been used in the calculation. Although the agreement with the calculations of columns one and two is improved, serious discrepancy still exists and the improvement which has been made is at the expense of much more computing time (six modes as opposed to three modes).

Table 2 shows further comparisons for the same ionospheres used in Table 1. Columns two, three and four show results for the total mode conversion coefficients for Model II (based on equations (16) and (17)). Column two gives results obtained using three modes for the truncated set, column three gives results using four modes and column four gives results using six modes. The significant feature is the stability of the solutions with mode truncation. For example, mode sum plots based on columns two and four would be indistinguishable.

In columns two and three of Table 3 are given results for the idealized ionosphere used in generating Tables 1 and 2 (except that $h_1 = 90$ km and $h_2 = 70$ km) as well as results for an abrupt transition between a nighttime exponential profile ($\beta = 0.5$ km^{-1}, $h_1 = 86$ km in the notation of Wait and Spies) and a daytime exponential profile ($\beta = 0.5$ km^{-1}, $h_2 = 70$ km). The latter results apply to propagation along the geomagnetic equator. The first and third columns give results including reflections (Model II) via (16) and (17). Observe that the application of the latter to the anisotropic case involves the assumption of reciprocity (we do not believe, however, that our conclusion about the unimportance

TABLE 2

$\omega_r = 2 \times 10^5$ SEC^{-1} $h_1 = 70$km $h_2 = 90$km $f = 20$kHz

MODE CONVERSION COEFFICIENTS

				WAIT	3 MODES XMTR MODEL II	4 MODES XMTR MODEL II	6 MODES XMTR MODEL II
J	1	K	1	0.4680 $\angle$ .0686	0.4730 $\angle$ .0614	0.4729 $\angle$ .0614	0.4728 $\angle$ .0612
J	1	K	2	0.1247 $\angle$ 3.2312	0.1242 $\angle$ -3.0792	0.1242 $\angle$ -3.0792	0.1240 $\angle$ -3.0801
J	1	K	3	0.0808 $\angle$ .0532	0.0765 $\angle$ -.0064	0.0764 $\angle$ -.0064	0.0762 $\angle$ -.0091
J	2	K	1	0.6552 $\angle$ -.0696	0.6603 $\angle$ -.0644	0.6603 $\angle$ -.0643	0.6606 $\angle$ -.0640
J	2	K	2	0.6366 $\angle$ .0078	0.6334 $\angle$ -.0116	0.6333 $\angle$ -.0116	0.6330 $\angle$ -.01218
J	2	K	3	0.2432 $\angle$ 3.1438	0.2295 $\angle$ 3.0914	0.2294 $\angle$ 3.0913	0.2287 $\angle$ 3.0887
J	3	K	1	0.1595 $\angle$ 3.0125	0.1570 $\angle$ 3.0476	0.1571 $\angle$ 3.0477	0.1674 $\angle$ 3.0498
J	3	K	2	0.5523 $\angle$ .0227	0.5692 $\angle$ 0.0290	0.5693 $\angle$ .0290	0.5697 $\angle$ .0299
J	3	K	3	0.4464 $\angle$ -.0645	0.4358 $\angle$ -0.0948	0.4357 $\angle$ -.0947	0.4350 $\angle$ -.0970

TABLE 3

	f = 20 kHz; ω_r = 2×10^5 SEC^{-1}, h_1 = 90km, h_2 = 70km; MODE CONVERSION COEFFICIENTS		f = 19.8 kHz; β = 0.5km^{-1}, h_1 = 86km, h_2 = 70km, DIP = 0, Az = 90°; MODE CONVERSION COEFFICIENTS	
	3 MODES, XMTR, MODEL II	3 MODES, XMTR, MODEL III	6 MODES, XMTR, MODEL II	6 MODES, XMTR, MODEL III
J = 1 K = 1	1.5194 $\angle$ -.0496	1.5174 $\angle$ -.0495	1.4477 $\angle$ .0073	1.4457 $\angle$ .0072
J = 1 K = 2	0.3981 $\angle$ .0355	0.3991 $\angle$ .0358	.4437 $\angle$ .1056	.4448 $\angle$ .1055
J = 1 K = 3	0.1070 $\angle$ -3.1172	0.1083 $\angle$ -3.1142	.0931 $\angle$ 3.0539	.0941 $\angle$ 3.0538
J = 2 K = 1	0.7940 $\angle$ 2.9808	0.7882 $\angle$ 2.9804	.6852 $\angle$ -3.1132	.6799 $\angle$ -3.114
J = 2 K = 2	0.7600 $\angle$ -.0239	0.7572 $\angle$ -.0245	.7272 $\angle$ -.0649	.7243 $\angle$ -.0654
J = 2 K = 3	0.7256 $\angle$ .0351	0.7294 $\angle$ .0362	.7957 $\angle$ .0722	.7987 $\angle$ .0716
J = 3 K = 1	0.4551 $\angle$ -.2116	0.4457 $\angle$ -.2128	.4197 $\angle$ .0410	.4103 $\angle$ .0396
J = 3 K = 2	0.2563 $\angle$ 3.0970	0.2516 $\angle$ 3.0947	.2409 $\angle$ -3.1382	.2363 $\angle$ -3.1397
J = 3 K = 3	0.5171 $\angle$ -.0708	0.5111 $\angle$ -.0741	.4519 $\angle$ -.1794	.4469 $\angle$ -.1809

of reflections in this case is contingent upon this assumption). Columns two and four give results with reflections ignored (Model III). Comparison of columns one and two as well as columns three and four suggests the degree to which reflections may be expected to influence mode conversion coefficients when propagating across the terminator (XTMR in the night region). The differences are again inconsequential in the sense that the mode sum plots with or without reflections would be identical for all practical purposes. Thus we conclude that as far as mode conversion is concerned, reflections can be ignored when treating propagation across the terminator in the ambient guide. We should point out that the magnitude of A_{11} is greater than unity because of the compression of the field which occurs in propagating from the night to the day region. Also, observe the close correspondence between the total conversion coefficients for the homogeneous isotropic ionospheres and the exponential ionospheres.

The remaining illustrations, except for Figures 8 and 9 where some results for Model I are included, are based on Model III (i.e. reflections are neglected). In Figures 1 through 6 mode sum plots based on mode conversion and the well known WKB approximation are shown.

Figure 1 illustrates the difference between the WKB result[9] and the mode conversion result for an abrupt, $\Delta D = 0$, transition located at D = 1000 km from the transmitter. The transmitter is in the nighttime portion of the guide. Exponential $\beta = 0.5$ km^{-1} profiles (notation Wait and Spies[10]) are assumed for both the night ($h_1 = 86$ km) and day ($h_2 = 70$ km) segments and propagation at and parallel to the geomagnetic

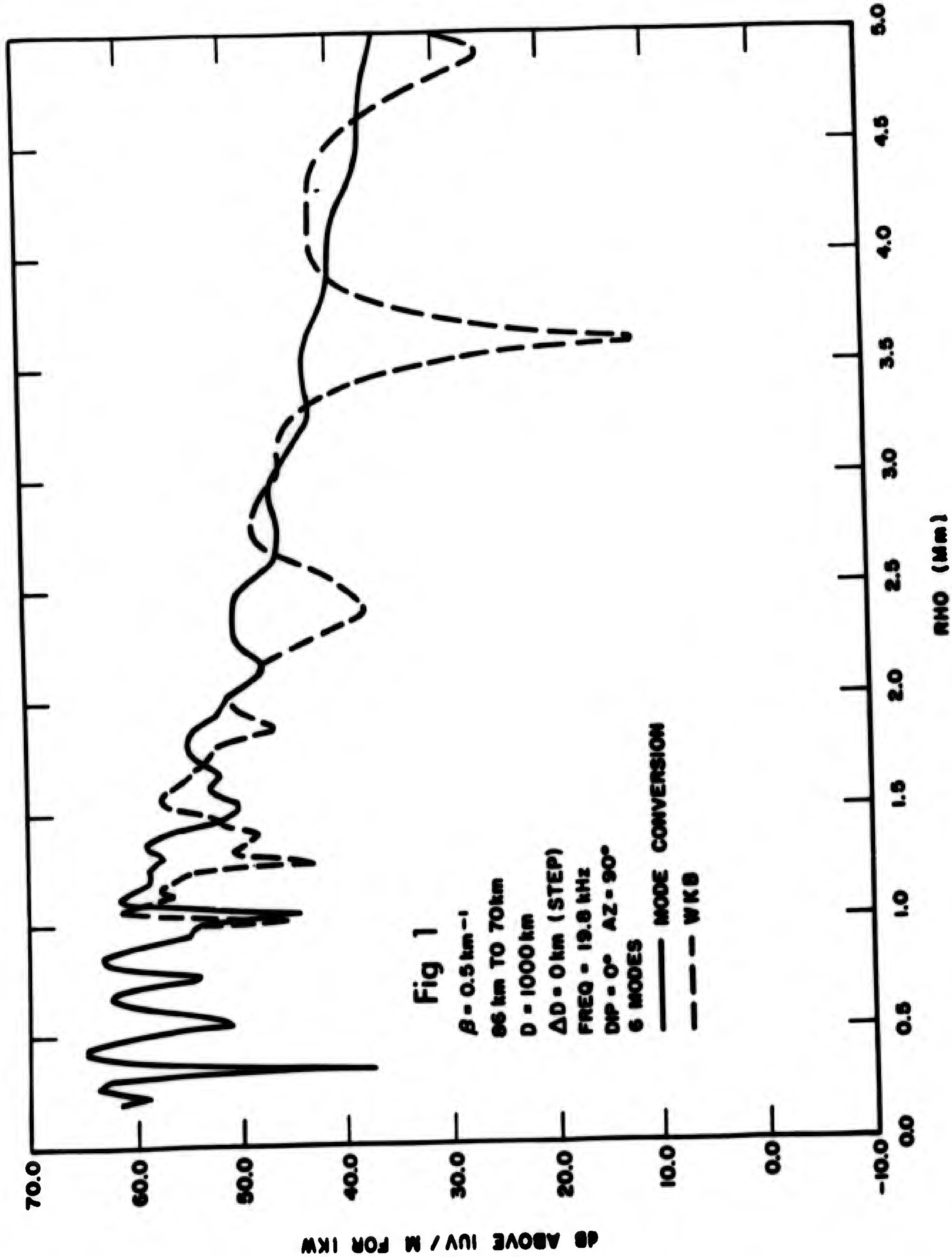
Fig 1
β = 0.5 km⁻¹
86 km TO 70km
D = 1000km
ΔD = 0km (STEP)
FREQ = 19.8 kHz
DIP = 0° AZ = 90°
6 MODES
MODE CONVERSION
WKB
RHO (Mm)
dB ABOVE 1UV / M FOR 1KW
0.0
0.5
1.0
1.5
2.0
2.5
3.0
3.5
4.0
4.5
5.0
70.0
60.0
50.0
40.0
30.0
20.0
10.0
0.0
-10.0

equator is assumed. The smoothing of the mode conversion result beyond about two megameters is due to mode one being wiped out at the junction. This feature is a direct consequence of the terminator being located at a point where modes one and three destructively interfere. If, for example, the transition were moved to a distance of 1500 km from the transmitter strong interference between modes one and two would be manifest in the mode sum plot.

Figure 2 shows the comparison between WKB and mode conversion results for a transition thickness of $\Delta D =$ 500 km with the beginning of the transition at D = 1000 km from the transmitter. The transmitter is in the nighttime portion of the guide. The night and day segments of the path and the propagation path are the same as in Figure 1. The parameter h which comes into the description of the ionospheric profile has been assumed to vary linearly between a height of 86 km and a height of 70 km. Ten slabs have been used in the calculation so that forty height gains are involved in the computation. The mode conversion plot beyond two megameters, unlike Figure 1, shows in this case strong interference between modes one and two. This is because modes one and three are not in antiphase over the entire region in which conversion occurs.

Figure 3 shows the same data as the previous figure except that the transition thickness has been increased to $\Delta D =$ 1000 km. A gradual evolution to the WKB result is evidenced as the transition thickness changes from the abrupt case to the case of a 1000 km transition thickness although even in the latter case the difference between the WKB result and the mode conversion result is not trivial.

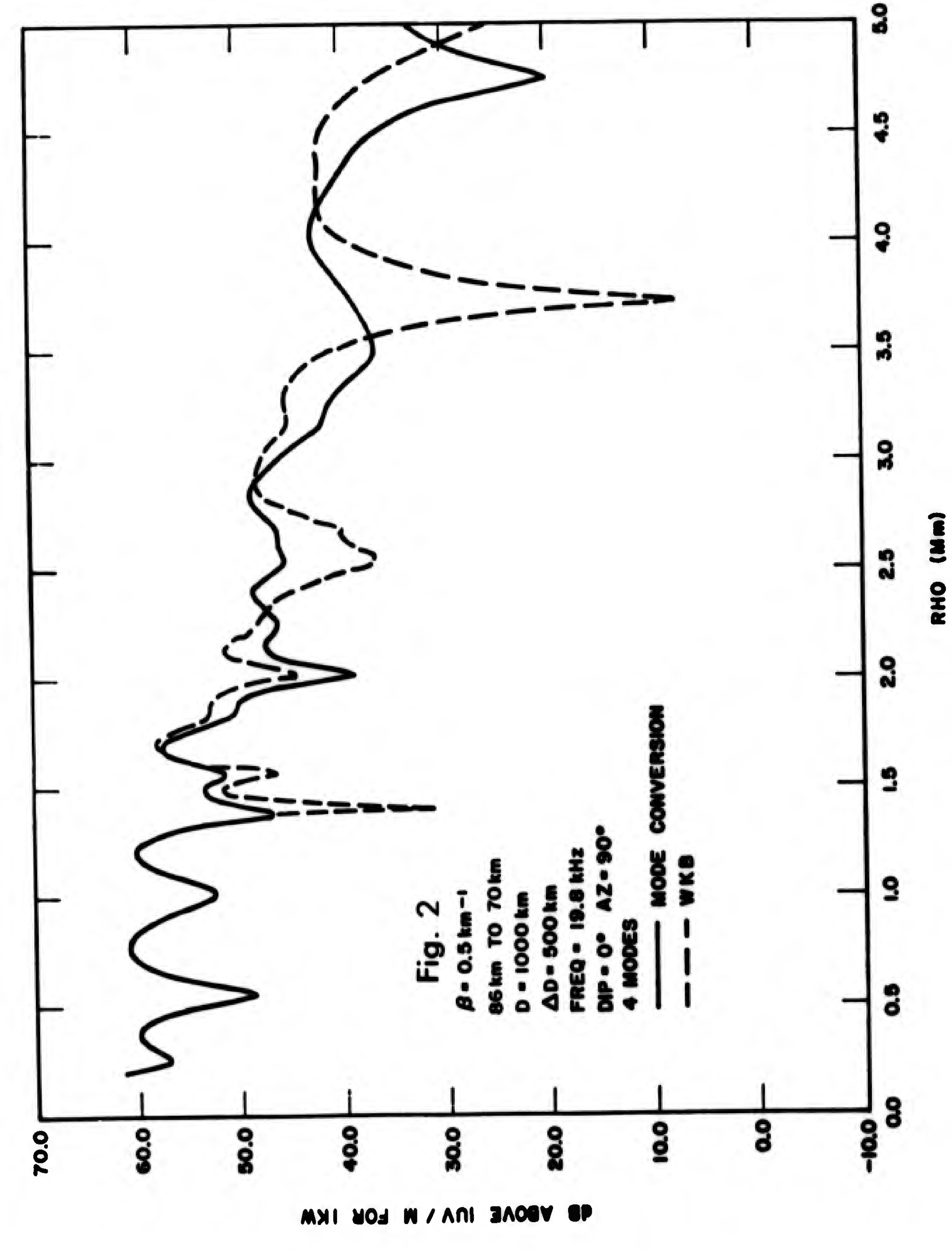
Fig. 2
β = 0.5 km⁻¹
86 km TO 70 km
D = 1000 km
ΔD = 500 km
FREQ = 19.8 kHz
DIP = 0° AZ = 90°
4 MODES
MODE CONVERSION
WKB
RHO (Mm)
dB ABOVE 1UV / M FOR 1KW
70.0
60.0
50.0
40.0
30.0
20.0
10.0
0.0
-10.0
0.0
0.5
1.0
1.5
2.0
2.5
3.0
3.5
4.0
4.5
5.0

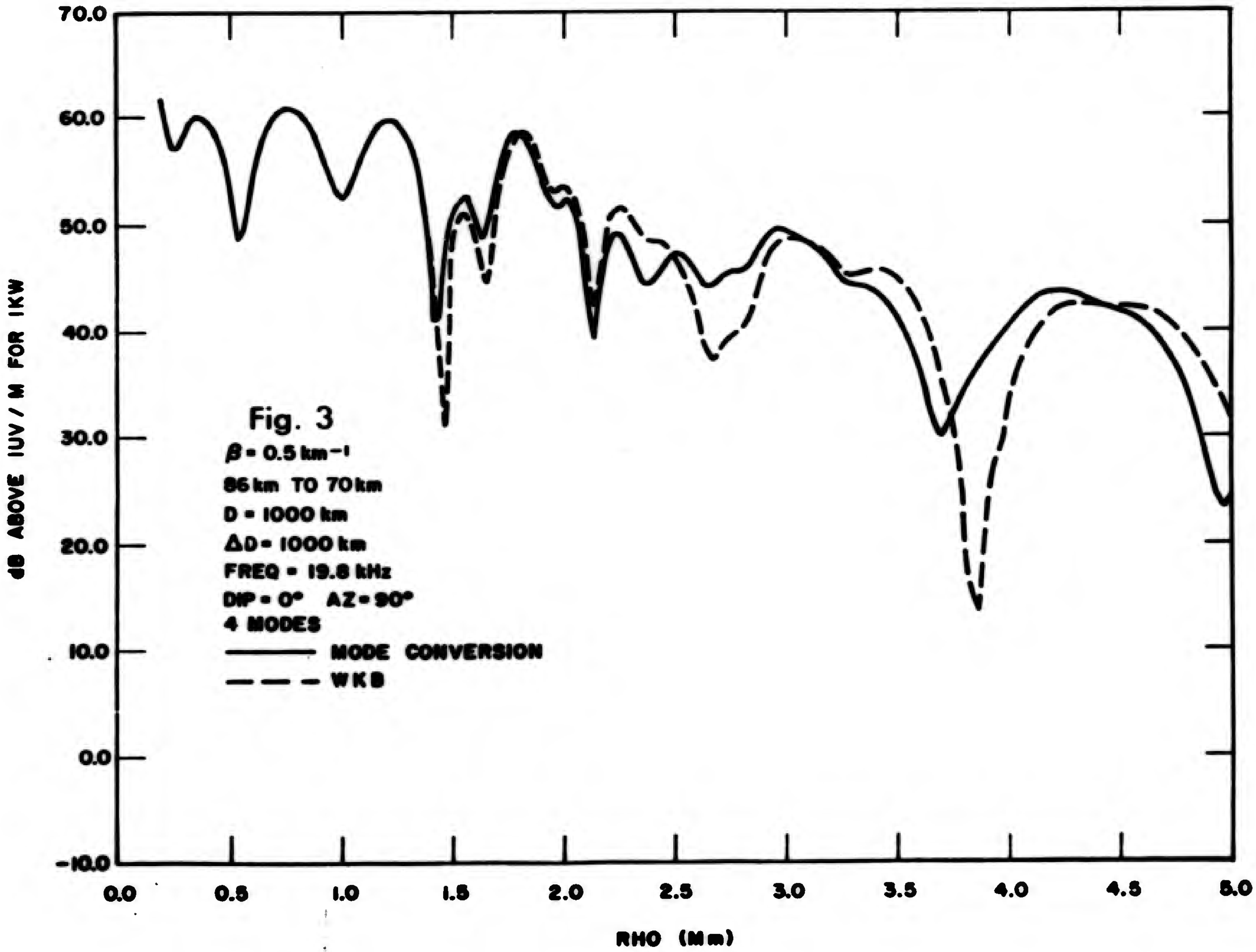
Fig. 3
β = 0.5 km^{-1}
86 km TO 70 km
D = 1000 km
ΔD = 1000 km
FREQ = 19.8 kHz
DIP = 0° AZ = 90°
4 MODES
MODE CONVERSION
WKB
dB ABOVE 1UV / M FOR 1KW
70.0
60.0
50.0
40.0
30.0
20.0
10.0
0.0
-10.0
0.0
0.5
1.0
1.5
2.0
2.5
3.0
3.5
4.0
4.5
5.0
RHO (Mm)

The difference between the WKB and mode conversion results is less dramatic for the case of the XTMR in the daytime portion of the guide. This is shown in Figure 4, which is a plot for the 1000 km thickness with the transmitter in the daytime side. In this case the WKB and mode conversion results are very similar.

The previous figures applied to the case of propagation along the geomagnetic equator. As an example of a more general dip angle, Figure 5 shows results for a hypothetical sea water to ice boundary, with the boundary at 1000 km from the transmitter (which is in the water portion of the guide). Only in proximity of the boundary do the mode conversion and WKB results differ significantly. The mode conversion result somewhat beyond the boundary gives a smaller signal strength than the WKB result. This despite the fact that the sea water-ice boundary is at a point where modes one and two constructively interfere. This is because the phasor resultant for mode one obtained from the direct conversion (A_{11} = (.078, - .570)) and the conversion from mode two to one (A_{12} = (-.183, .126)) is less than if there had been no conversion from mode two to one. For the case of a boundary somewhat more removed from the transmitter (D = 2500 km), Figure 6 shows the mode conversion and WKB results are essentially identical somewhat beyond the boundary. The reason for this is that the energy in mode two is sufficiently reduced at 2500 km that the interference phenomena mentioned above is insignificant.

We conclude this section with a series of comparisons with the experimental modeling results generated by the American Nucleonics Corporation.

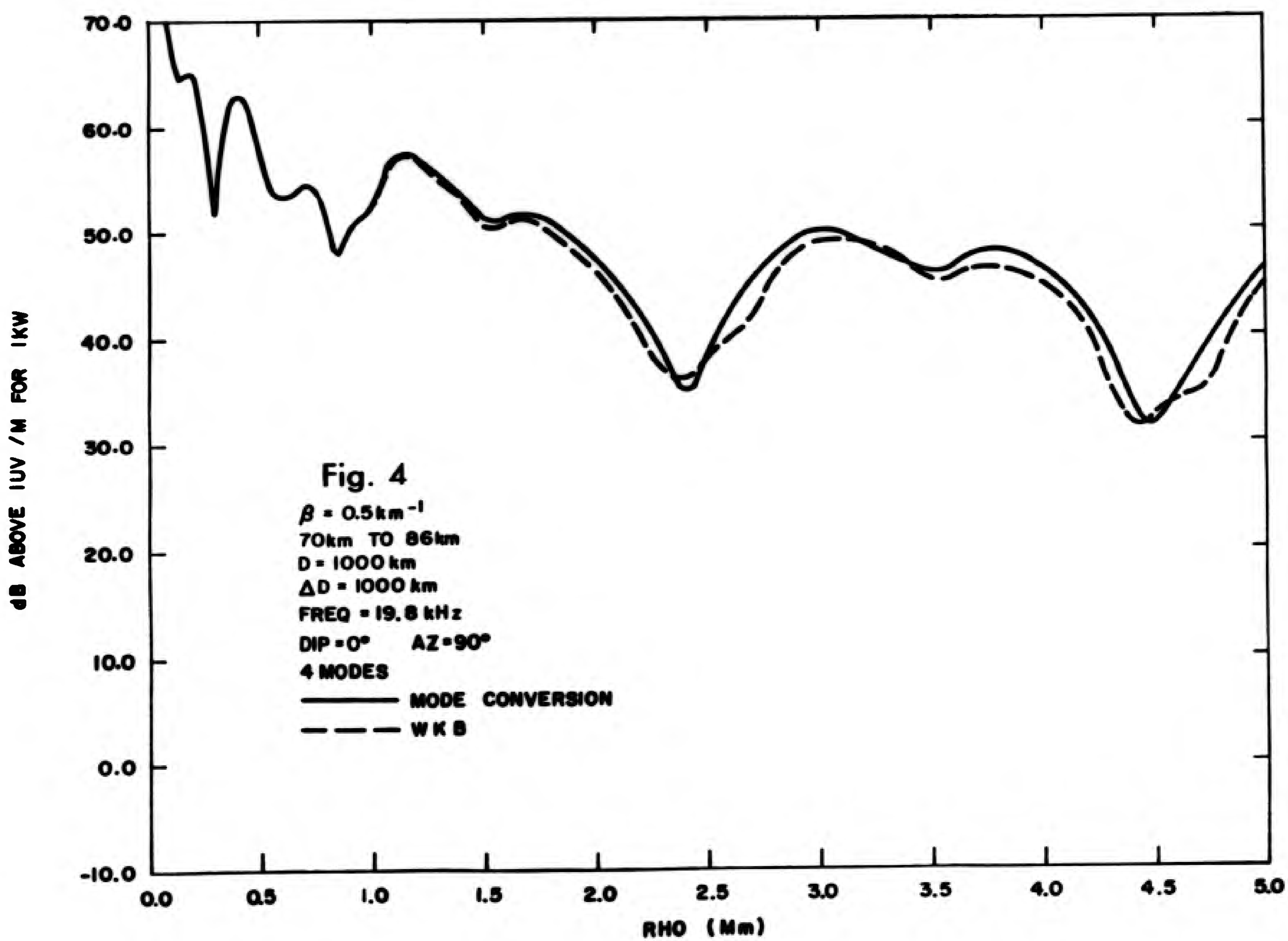
Fig. 4
β = 0.5km⁻¹
70km TO 86km
D = 1000 km
ΔD = 1000 km
FREQ = 19.8 kHz
DIP = 0°   AZ = 90°
4 MODES
MODE CONVERSION
W K B
70.0
60.0
50.0
40.0
30.0
20.0
10.0
0.0
-10.0
dB ABOVE 1UV / M FOR 1KW
0.0
0.5
1.0
1.5
2.0
2.5
3.0
3.5
4.0
4.5
5.0
RHO (Mm)

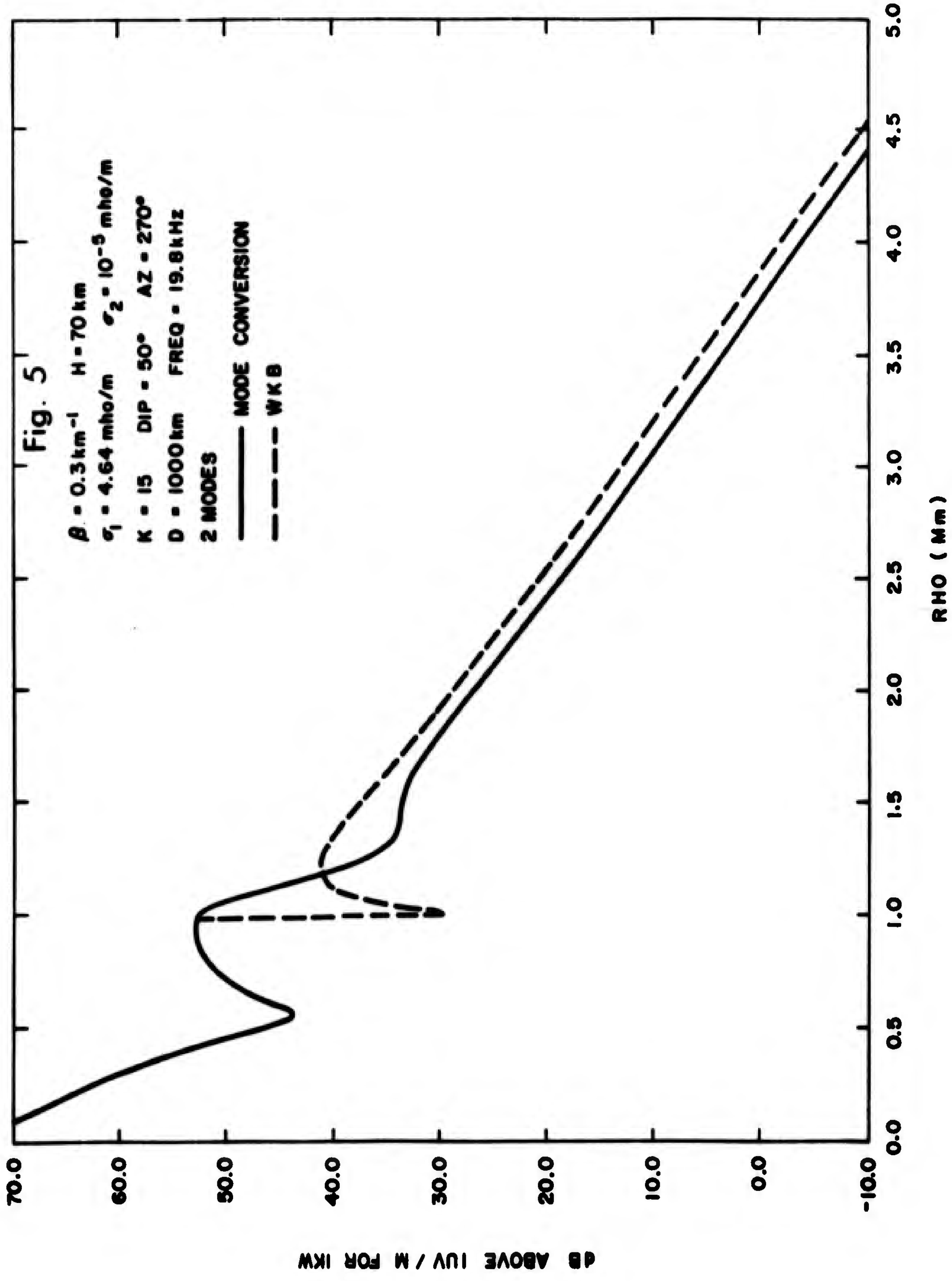
β = 0.3 km^{-1} H = 70 km
σ_1 = 4.64 mho/m σ_2 = 10^{-5} mho/m
K = 15 DIP = 50° AZ = 270°
D = 1000 km FREQ = 19.8 kHz
2 MODES
MODE CONVERSION
WKB
70.0
60.0
50.0
40.0
30.0
20.0
10.0
0.0
-10.0
dB ABOVE 1UV / M FOR 1KW
0.0
0.5
1.0
1.5
2.0
2.5
3.0
3.5
4.0
4.5
5.0
RHO (Mm)

Fig. 5

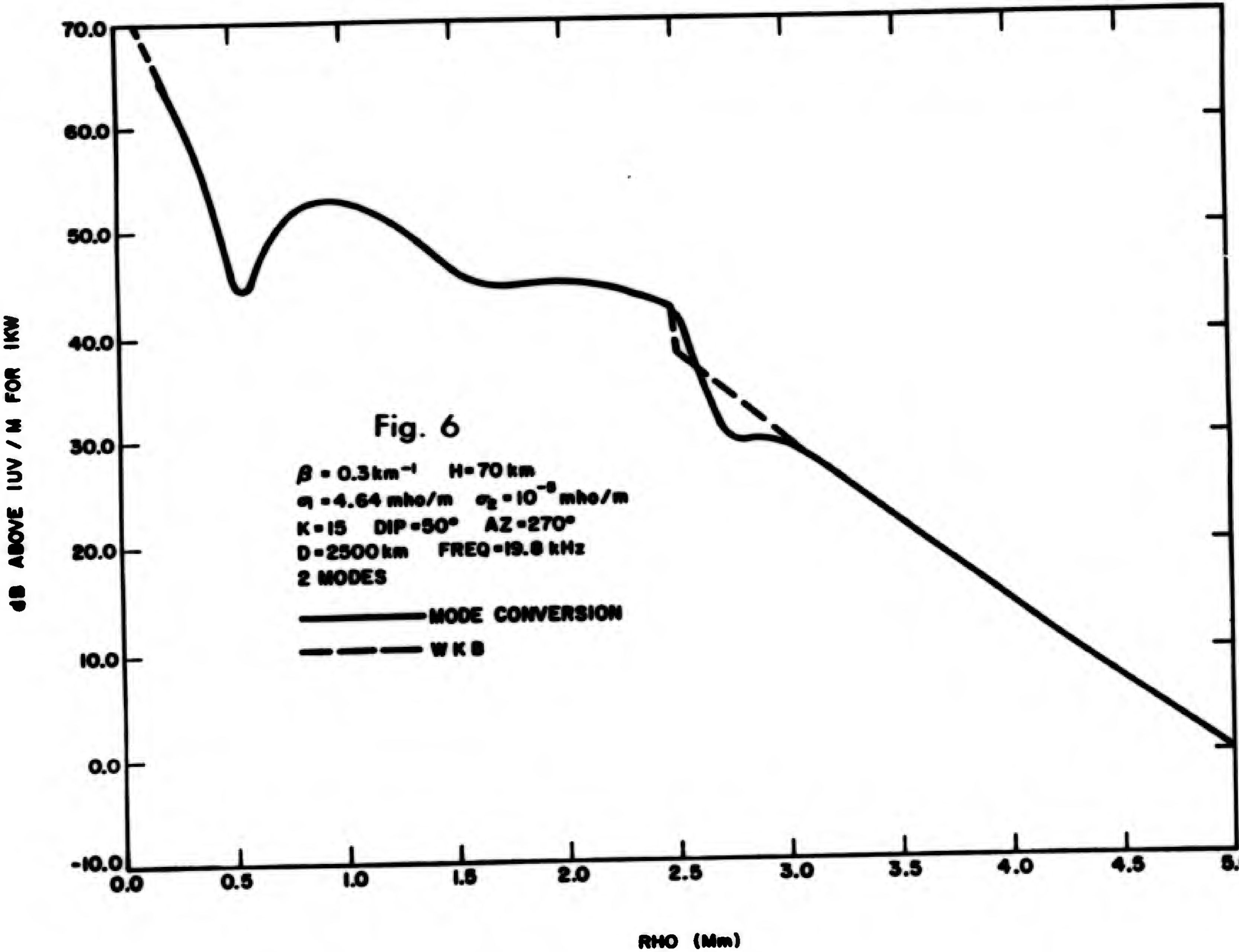
β = 0.3 km⁻¹ H = 70 km
σ1 = 4.64 mho/m σ2 = 10⁻⁵ mho/m
K = 15 DIP = 50° AZ = 270°
D = 2500 km FREQ = 19.8 kHz
2 MODES
MODE CONVERSION
W K B
dB ABOVE 1UV / M FOR 1KW
RHO (Mm)
70.0
60.0
50.0
40.0
30.0
20.0
10.0
0.0
-10.0
0.0
0.5
1.0
1.5
2.0
2.5
3.0
3.5
4.0
4.5
5.0

Fig. 6

Figure 7 shows a series of perturbations considered by American Nucleonics.[2] The perturbations extend uniformly across the guide. The transmitter is a 20 dB horn located 400 km to the left of the leading edge of the perturbation. The scaled frequency is 20 kHz. The square of the index of refraction of the dielectric used to simulate the ionosphere is

$$n^2 = 2.16\,(1.0 - 0.662j) \tag{18}$$

Shown in Figure 8 is a comparison between the theoretical and the experimental modeling results for the sharpest perturbation. The theoretical results are for point dipole excitation for Models I and III. It is evident that Model III does a superior job of predicting the magnitude of the dip which occurs in the neighborhood of 100 km. Apart from a seeming displacement between the experimental and theoretical results in the 500 to 1500 km range the theoretical results for Model III are in excellent agreement with the experimental results. Part of this displacement may result from the difference in excitation between a point dipole and a 20 dB horn. The experimental results in the neighborhood of 1500 and 2500 km show evidence of a higher order mode structure. The theoretical results have been generated using two modes and would be essentially unchanged in a three mode calculation because the attenuation rate for mode three is ≈26 dB per megameter.

Shown in Figure 9 is a comparison between theoretical results and the experimental modeling results for the perturbation labeled 2 in

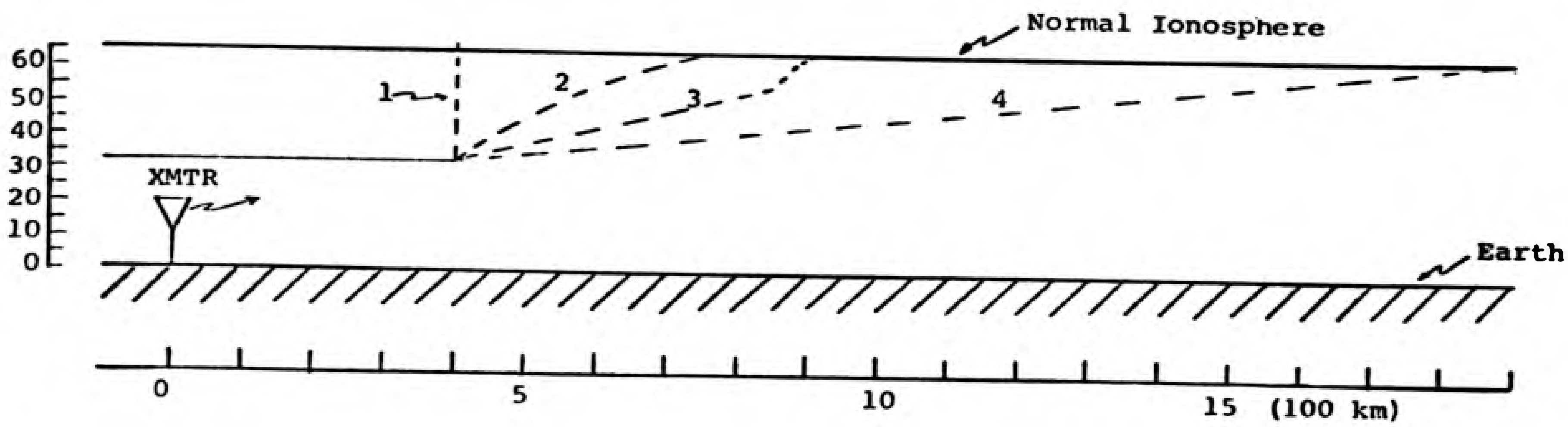

Figure 7 Ionospheric Configurations. All disturbed configurations begin with the ionosphere depressed to a height of 32.5 km. The transition to the normal ionosphere (h = 65 km) begins at a distance of 400 km from the transmitter (XMTR). The severity of the transition decreases with increasing number.

(Taken from American Nucleonics Corporation - TM32-18)

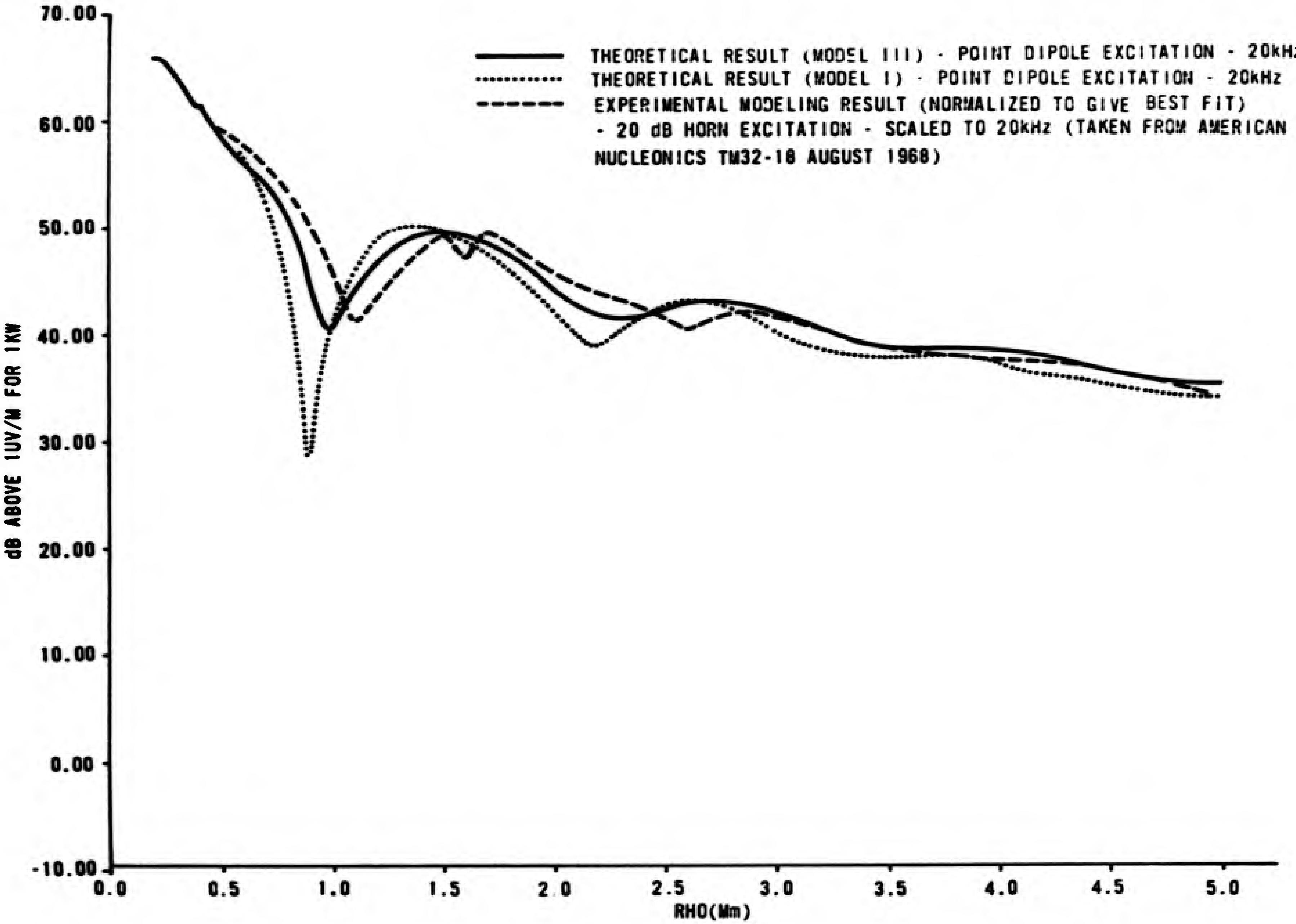

FIGURE 8. PERTURBATION 1

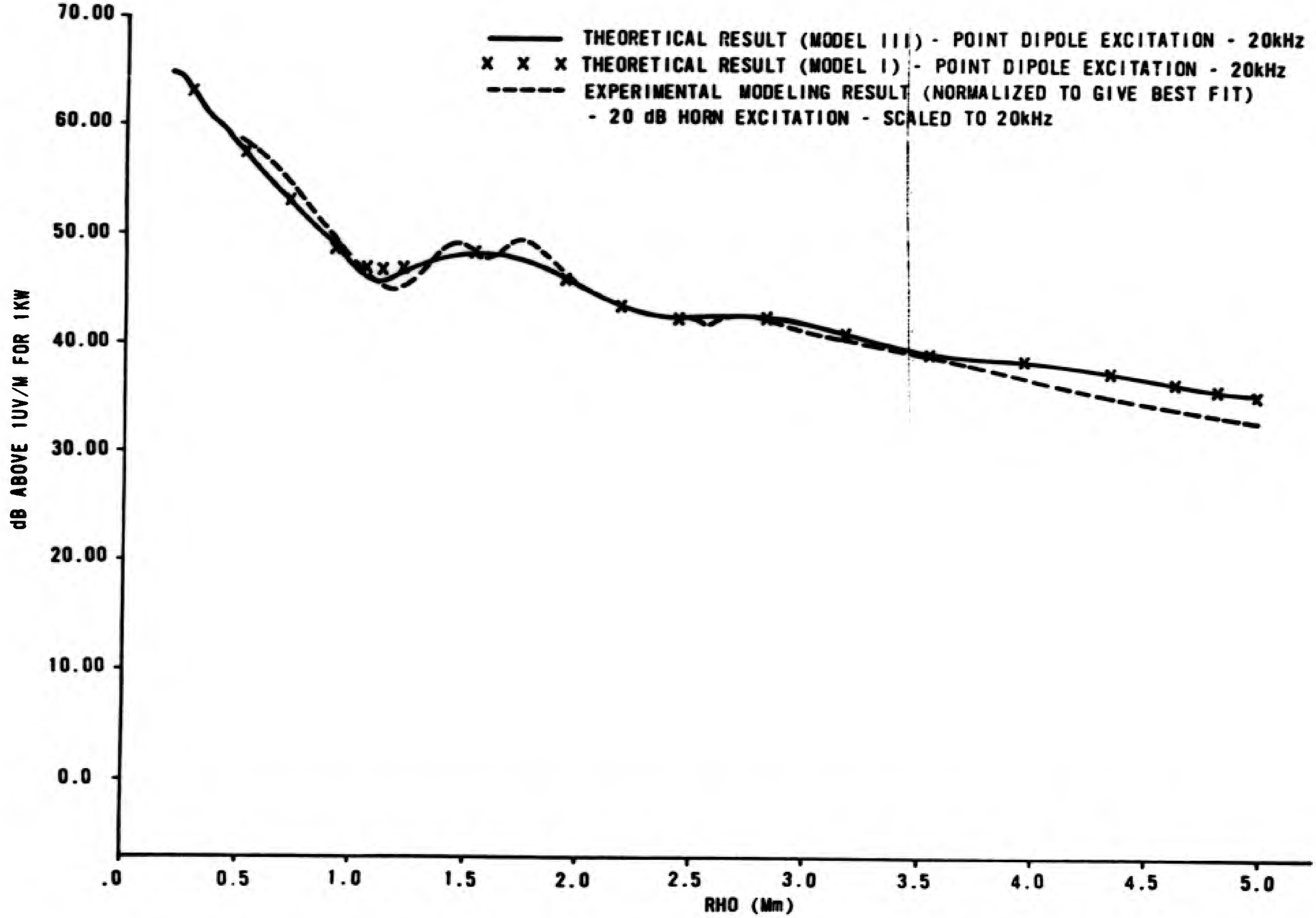

FIGURE 9. PERTURBATION 2

Figure 7. Again the theoretical results are for point dipole excitation. In addition to the difference in source excitation there is the difference due to the fact that an eight-slab model has been used to numerically simulate the perturbation. This eight-slab model has the following description

M	x(m) - km	h(m) - km
1	725	65
2	620	60
3	560	55
4	520	50
5	480	45
6	440	40
7	400	35
8		32.5

In this case the theoretical results based on Models I and III are very nearly identical. The overall agreement between the measured and theoretical results is quite remarkable considering the aforementioned differences between the experimental and numerical models.

Shown in Figure 10 is a pathological disturbance which has been experimentally modeled by American Nucleonics.[3] The ionosphere directly over the transmitter is undisturbed. At a scaled distance of 500 km from the transmitter the ionospheric depression begins. The depression is in the form of a wedge section which extends uniformly across the waveguide. The ionospheric reflection height decreases

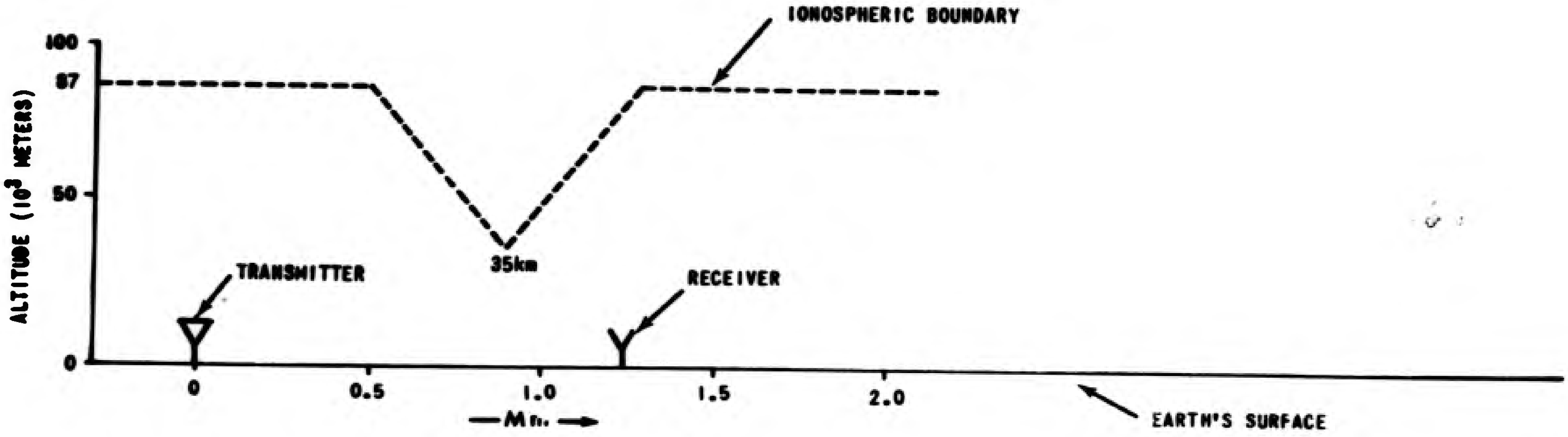

FIGURE 10. OUTLINE OF THE PERTURBED IONOSPHERIC MODEL ALONG THE PROPAGATION PATH (TAKEN FROM AMERICAN NUCLEONICS TM32-22 MARCH 1970 - PREPARED FOR DASA)

linearly with distance from 87 km to 35 km. The minimum occurs at 900 km. The reflection height then returns linearly to 87 km at a scaled 1300 km from the transmitter. The entire disturbed region covers a distance of 800 km. The length of the dipole transmitter scales to 3.55 km and the dipole receiver to 6 km.

Shown in Figure 11 is a comparison of the numerical and experimental modeling results for the unperturbed (h = 87 km) guide. Three modes with attenuations of 2.10, 3.96, 10.74 dB per megameter have been used in the calculations. The discrepancy in the depth of the null at about 500 km could be due to minor differences in the excitation factors since neither the transmitter nor the receiver are point dipoles. Agreement between the numerical and experimental results is quite good out to about 3300 km. The discrepancy at distances beyond 3300 km occurs in a region of rather weak signal to noise ratio. Again there is evidence in the experimental result around 1900 km of extraneous reflections or additional modal interference. It is very unlikely that this structure would show up in the numerical modeling even if a fourth order mode had been included.

The slab model used for numerical simulation of the triangular depression is shown in Figure 12. It is clearly a rather crude approximation with 10 km height changes occurring between most of the adjacent slabs. Despite the coarseness of the model, however, Figure 13 shows that the numerical and theoretical mode conversion curves are in rather good agreement out to about 4000 km. The disparity beyond

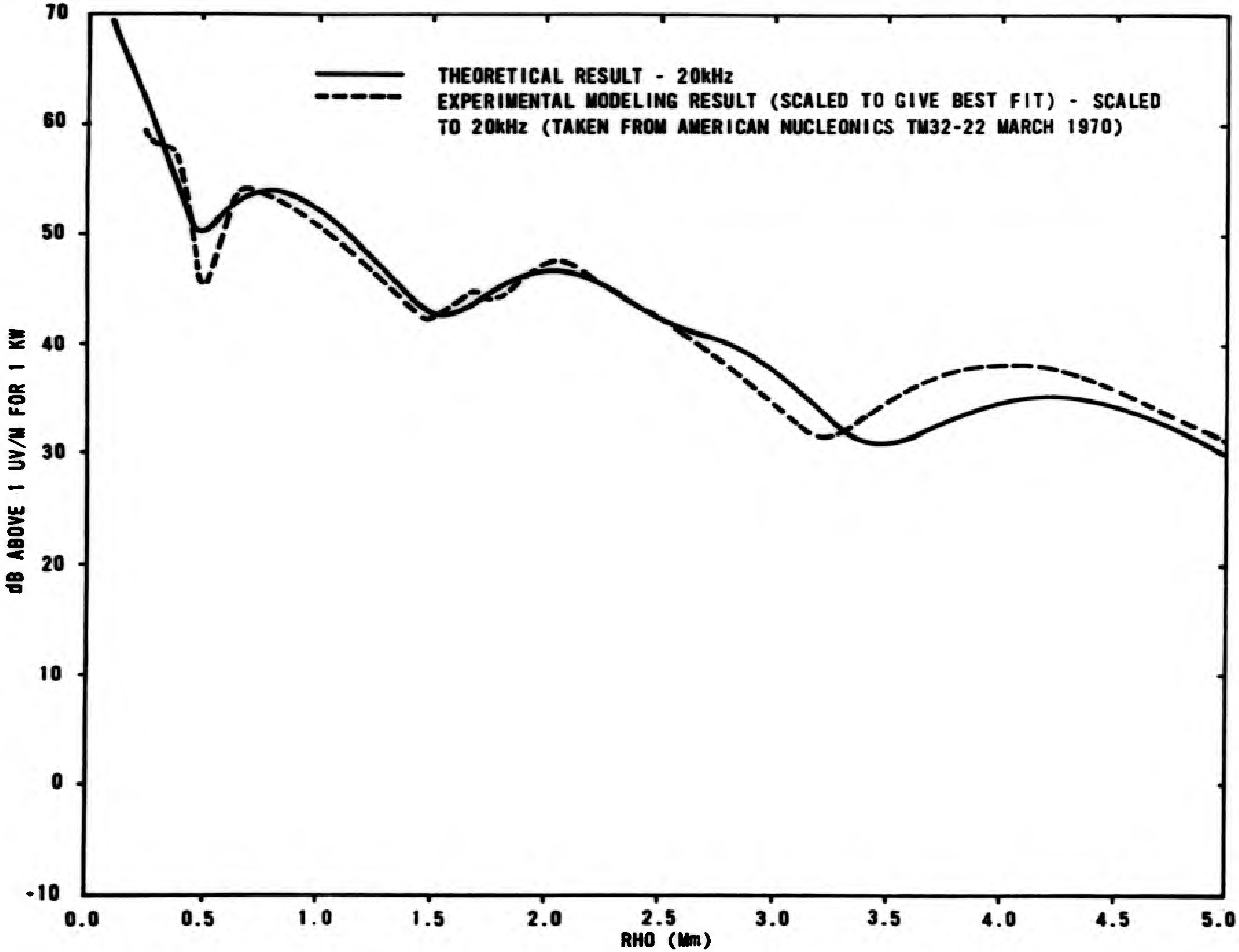

FIGURE 11. DIPOLE EXCITATION - UNPERTURBED (h = 87 km)

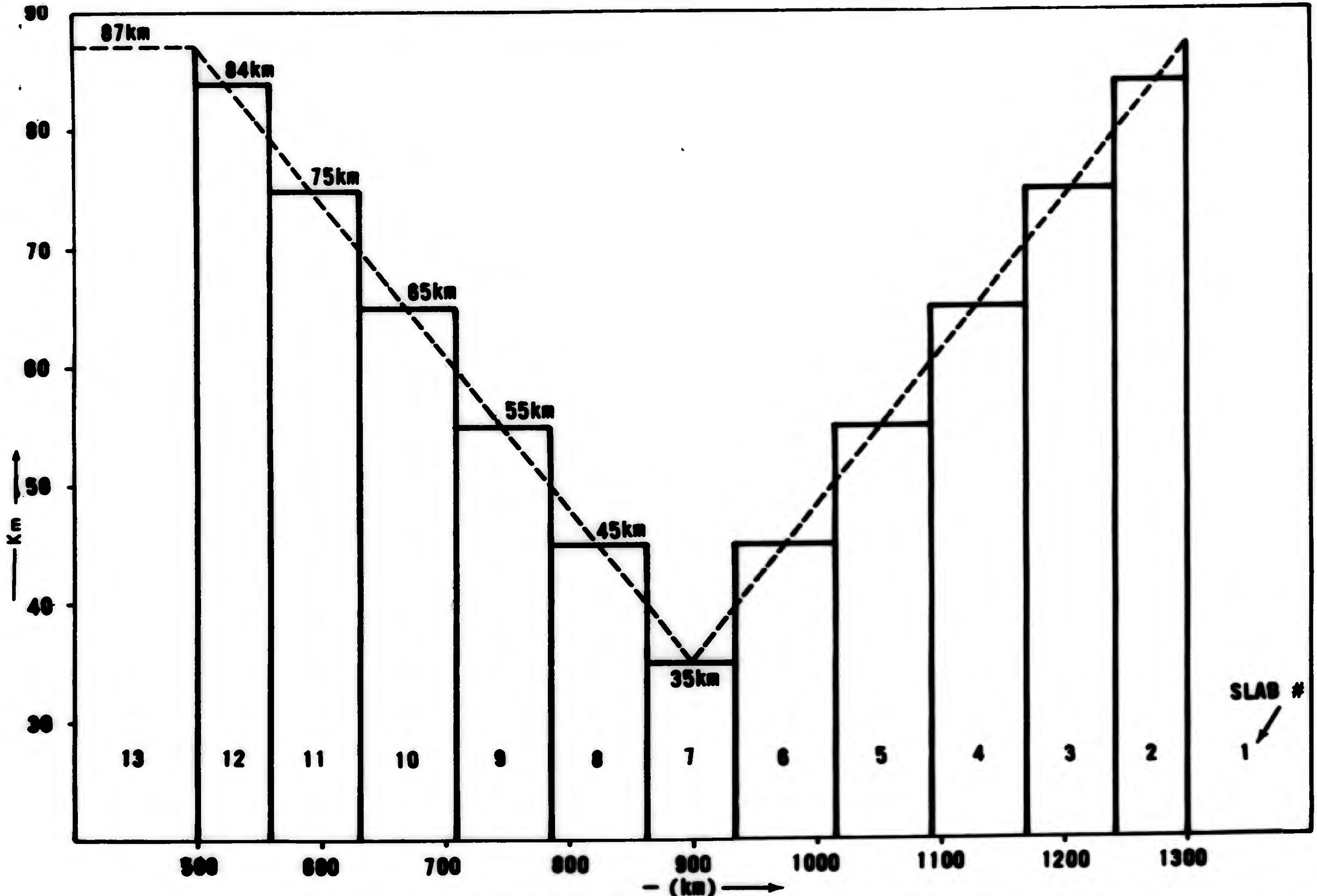

FIGURE 12. MODEL FOR NUMERICAL SIMULATION OF TRIANGULAR DEPRESSION

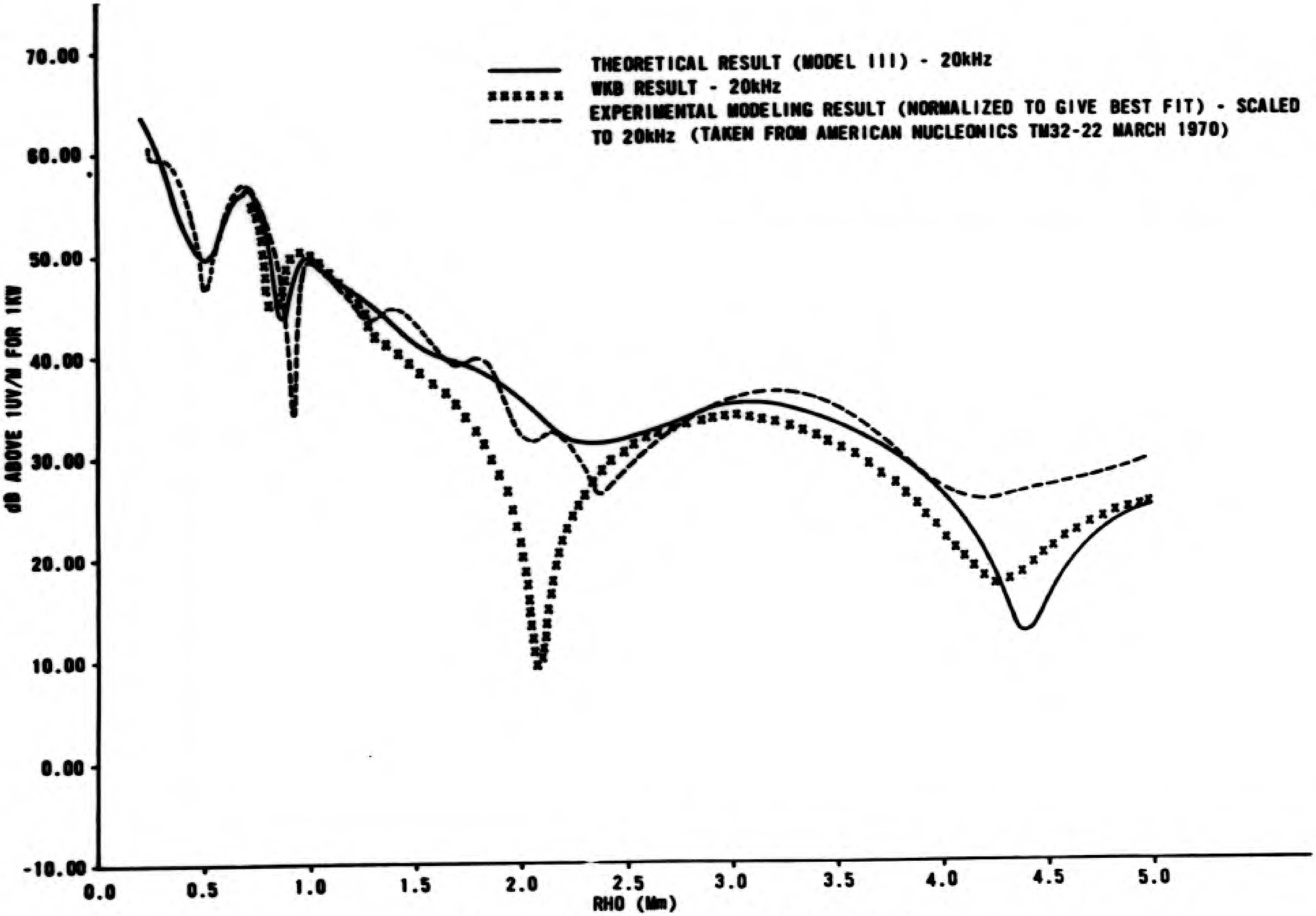

FIGURE 13. DIPOLE EXCITATION TRIANGULAR PERTURBATION

4000 km could easily be due to weak signal to noise ratio. Shown also in Figure 13 is the WKB result for the triangular depression. Observe that it predicts at about 2100 km a field strength which is about 20 dB below both the numerical and experimental (normalized to give best fit) results. Also, it should be observed that even in this pathological case there is no clear cut evidence that reflections play a significant role.

IV. CONCLUSIONS

Table 1 and Figure 8 demonstrate that the preferred method for handling the mode conversion problem is to decompose a unit amplitude wave incident on the junction into a truncated set of modes passing through and emerging from the junction rather than, as was suggested in reference one, adjusting the strengths of a truncated set of modes in such a way as to synthesize a unit amplitude wave in a given mode emerging from the transition region. The reason for this is that, apparently, the latter approach places the unrealistic constraint on the problem that only conversion between the truncated set of modes occurs. If the transition region is sufficiently gradual this constraint does not appear to seriously impair the results (Figure 10). Table 3 indicates the unimportance of reflections on the total mode conversion coefficients when propagating across the terminator. In fact for the pathological case study shown in Figure 10 there is no clear cut evidence that reflections are significant even in this case (Figure 13).

Figure 3 shows that significant departure between mode conversion and WKB mode sums can occur even for transition thicknesses as large as 1000 km.

REFERENCES

1. Pappert, R. A., and R. R. Smith, "Mode conversion program for an inhomogeneous isotropic ionosphere," Naval Electronics Laboratory Center Interim Report No. 701 for DASA, April 1970.

2. Schwartz, K., "The effect of different ionospheric transition zones on propagation at 20 kHz," American Nucleonics Corporation TM 32-18 for DASA, August 1968.

3. Schwartz, K., "VLF propagation with a highly disturbed ionosphere-a test case for digital computer simulation technique," American Nucleonics Corporation TM 32-22 for DASA, March 1970.

4. Pappert, R. A., and R. R. Smith, "Orthogonality of VLF height gains in the earth ionosphere waveguide (submitted to Electronics Letters).

5. Sheddy, C. H., R. Pappert, Y. Gough and W. Moler, "A fortran program for mode constants in an earth-ionosphere waveguide," Naval Electronics Laboratory Center Interim Report No. 683 for DASA, May 1968.

6. Wait, J. R., "Mode conversion and refraction effects in the earth-ionosphere waveguide for VLF radio waves," Journal of Geophysical Research, Vol. 73, No. 11 (1968), pp 3537-3548.

7. Smith, R. R., "A program to compute ionospheric height gain functions and field strengths," Naval Electronics Laboratory Center Interim Report No. 711 for DASA, December 1970.

8. Henrici, P., "Elements of numerical analysis," Wiley, New York, London, Sydney (1964), pp 259-261.

9. Wait, J. R., "Two dimensional treatment of mode theory of propagation of VLF radio waves," Radio Science, Vol. 68D, No. 1, pp 81-93.

10. Wait, J. R. and K. P. Spies, "Influence of finite ground conductivity on the propagation of VLF radio waves, Radio Science, Vol. 69D, No. 10, pp 1359-1373.